

# A New Algorithm for Design and Optimize of Linear Synchronous Motors with DC Excitation

1<sup>st</sup> A. Fleming  
Dept. Electrical and Computer  
Engineering  
University of Carolina  
Carolina, USA  
a.fleming1010@gmail.com

2<sup>nd</sup> M. Zarei  
Dept. Electrical and Computer  
Engineering  
University of London  
London, England  
mehdi.zarreei@gmail.com

3<sup>rd</sup> V. Sezar  
Dept. Electrical and Computer  
Engineering  
University of Ankara  
Ankara, Turkey  
vol.sezar@gmail.com

**Abstract**—The Linear Synchronous Motor with DC Excitation is presented based on its steady-state equations. Until now, many methods based on solving the magnetic equations of the motor or using numerical methods have been presented in various types of research, and complex mathematical equations and time-consuming design are their main problems. In the proposed method, this type of motor has been designed using the electrical relations of the circuit of the Linear Synchronous Motor. Due to the simplicity of relationships and faster design, this method can be easily used in some topics, such as optimization that require repetition algorithms. For validation, the ©MATLAB has been used.

**Keywords**— Linear Motors (LMs), Linear Synchronous Motors (LSMs), DC Excitation, Finite Element Method (FEM), Optimization Algorithm

## I. INTRODUCTION

In the contemporary era, the achievement of linear motion is being considered due to its wide application in various industries, such as industrial automation systems, transportation, and military industries. Linear Motors (LMs) can be used for the linear motion because they have many advantages over Rotary Motors (RMs) and rotary-to-linear motion converters [1]. An LM is an Electric Motor (EM) whose stator and rotor are out of circular mode so that instead of producing rotational torque, it makes linear force longitudinally. The most common mode of operation is the Lorentz force operator; whose applied force is linearly proportional to the electric current and magnetic field. Many designs have been proposed for LMs, and they are divided into two main categories; high-speed and high-acceleration LMs [2].

A Linear Synchronous Motor (LSM) is a Linear motor in which the mechanical movement's speed equals the speed of the moving magnetic field. Typically, multi-phase AC synchronous motors are motors with DC electromagnetic excitation in which the moving force has two components; the first component is caused by the interaction of the traveling magnetic field with the DC magnetic field or the magnetic field generated by permanent magnets. The second component is also caused by the interaction of the traveling magnetic field with variable reluctance in the (d) and (q) axes [3-5].

The Linear Synchronous Motor is one of the types of LM. LSM is the linear counterpart of the Rotary Synchronous Motor in which the electrical power input to the machine is converted into mechanical work at their output by linear movement. High efficiency, high-power factor, and an internal magnetic source make LSM suitable for various applications [6].

In the previous research about LSM, various aspects such as modeling, design, and control have been investigated. Attempts to model the LSM led to models with complex mathematical relationships. Therefore, using these design models has limitations [7-8].

In this article, a method for modeling and designing an LSM with DC excitation will be presented. The main purpose of this article is to reduce the complexity of the design to achieve a suitable method for optimizing LSM. After introducing the structure of the LSM in section II, the model used for its design and calculations will be presented in section III. Then the design process will be presented in section IV. In section V, the validity of the obtained results will be evaluated using ©MATLAB, and finally, the summary and conclusions will be presented in section VI.

## II. STRUCTURE OF THE LSM

Figure 1 shows the general schematic of a one-way LSM with DC excitation. The primary motor consists of three-phase windings with an iron core along the movement path. Copper windings are placed in grooves embedded in the iron core. The movement path consists of two parts, one part is electrified, and the other is not electrified. The electrified section is selected to be five times the moving length on which the DC excitation is located (not specified in Figure 1) and is powered by a voltage source.

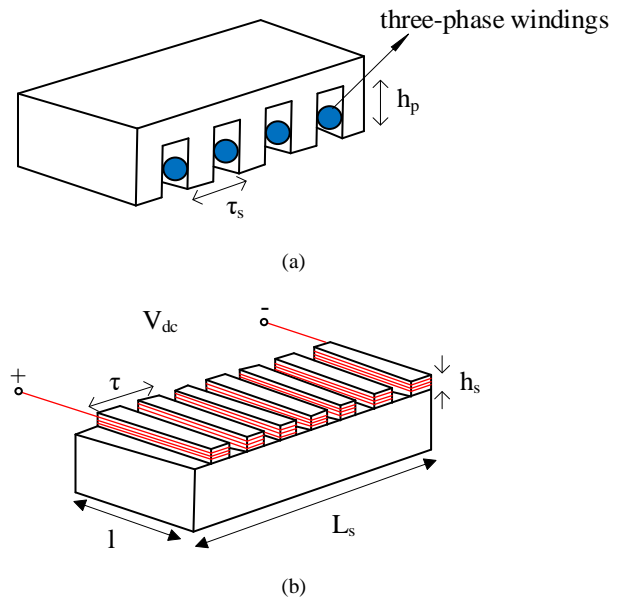


Fig. 1. Structure of the LSM: a) Primary (Part of Fix), b) Secondary (Part of moving)

The moving part of the motor consists of an iron core and DC excitation electromagnetic poles, which are placed on top of the primary. There is no physical contact between the secondary and the primary, and an air gap separates these two parts. Secondary (moving) windings are made of copper.

### III. PERFORMANCE AND MODELING OF THE LSM

To obtain a method for designing the LSM with DC excitation, the steady-state model of the motor is used. Therefore, in this section, the steady-state equations of the motor will be discussed.

#### A. Equations of the Steady-State

Based on the phasor diagram of the LSM excited by the salient pole, the input voltage will be calculated according to the following equation [9]:

$$\vec{V}_s = R_{ph}\vec{I}_s + X_{sd}\vec{I}_{sd} + jX_{sq}\vec{I}_{sq} + \vec{E}_f \quad (1)$$

The equations of the d and q axes are as follows:

$$V_s \sin \delta = -R_{ph}I_{sd} + X_{sq}I_{sq} \quad (2)$$

$$V_s \cos \delta = R_{ph}I_{sq} + X_{sd}I_{sd} + E_f \quad (3)$$

In the above relationship,  $V_s$  is the value of the stator's voltage, and  $I_s$  is the value of the current of the stator.  $I_{sd}$  and  $I_{sq}$  are the images of the  $I_s$  on the d and q axes. Also,  $E_f$  is the effective value of the no-load induced voltage on one phase of the stator windings due to DC excitation and this voltage will be expressed in the following.  $\delta$  is the load factor between  $V_s$  and  $E_f$ . Also,  $R_{ph}$  is the resistance of each primary phase,  $X_{sd}$  and  $X_{sq}$  are the reactance of the d and q axes, respectively, and are calculated from the following relationships [9]:

$$R_{ph} = \rho \frac{l_w}{A_w} \quad (4)$$

$$X_{sd} = X_{ph} + X_a + X_{sd} \quad (5)$$

$$X_{sq} = X_{ph} + X_a + X_{sq} \quad (6)$$

In the above equations,  $\rho$  is the specific resistance of the conductors used in the primary winding,  $l_w$  is the length of the primary winding, and  $A_w$  is the cross-section of the conductors.  $X_{ph}$  is the scattering reactance of each preliminary phase,  $X_a$  is the leakage reactance of the air gap,  $X_{sd}$  and  $X_{sq}$  are the magnetization reactance of the d-axis and q-axis, respectively. They can be calculated from the following relations [1].

$$X_{ph} = 2\mu_0\omega\left[\left(\lambda_s + \left(\frac{N_1}{N_2}\right)\lambda_d\right)l + \lambda_e l_{ec}\right] \frac{N_1 N_2}{pq} \quad (7)$$

$$X_a = \frac{6\mu_0\omega l(N_2 - N_1)}{\pi} \quad (8)$$

$$X_{sd} = \frac{6\mu_0\omega\tau l N_1^2}{\pi^2 k_c g_0} k_d \quad (9)$$

$$X_{sq} = \frac{k_q}{k_d} X_{sd} \quad (10)$$

In which,  $\mu_0$  is the magnetic permeability coefficient of air, and  $\omega$  is the initial angular frequency. Also,  $\lambda_s$ ,  $\lambda_d$  and  $\lambda_e$  are the specific magnetic conductivity of slot, differential, and end connections, respectively.  $N_1$  and  $N_2$  are the number of turns in the primary phase for the overlapping part with the moving part and the electrified part empty of moving, respectively. Also,  $l$  is the motor's width,  $l_{ec}$  is the length of end connections,

$p$  is the number of pole pairs,  $q$  is the number of slots in each phase,  $\tau$  is the pole pitch,  $g_0$  is the distance of air gap,  $k_c$  is the Carter coefficient,  $k_d$  and  $k_q$  are coefficients of the effect of the armature on the d-axis and q-axis, respectively, and can be calculated from the following equations [10]:

$$k_d = (\pi\alpha_p + \sin \pi\alpha_p)/\pi \quad (11)$$

$$k_q = (\pi\alpha_p - \sin \pi\alpha_p)/\pi \quad (12)$$

That,  $\alpha_p$  is the ratio of pole arc to pole pitch. Also,  $E_f$  can be calculated from the following equation [10]:

$$E_f = \sqrt{2}B_f l N_1 \omega_s \quad (13)$$

In the above relation  $B_f$  is the density of the flux of the air gap which caused by the excitation of DC.  $\omega_s$  is the synchronous speed. These parameters can be calculated by the following relations [10]:

$$\omega_s = 2\pi f \quad (14)$$

$$B_f = \frac{\mu_0 N_f I_f}{k_c g_0 (1 + k_{sat})} \quad (15)$$

Where,  $f$  is frequency,  $N_f$  is the number of turns of the DC excitation winding,  $I_f$  is the DC excitation current,  $k_{sat}$  is the coefficient of iron saturation. Also, we have:

$$I_f = \frac{V_{dc}}{R_f} \quad (16)$$

That,  $V_{dc}$  is the voltage of the DC excitation, and  $R_f$  is the excitation winding resistance.

#### B. Calculations of the Power, Force and Efficiency

By ignoring the core losses, the electromagnetic power can be calculated as follows [11]:

$$P_e = mV_s I_s \cos \varphi - mR_s I_s^2 \quad (17)$$

In which,  $m$  is the number of primary power supply phases and  $\cos \varphi$  is the input power factor. So, the electromagnetic force of the motor is obtained from the following equation:

$$F_e = \frac{P_e}{\omega_s} \quad (18)$$

Using the relations (2), (3), and (18), the electromagnetic force can be expressed as a function of the  $\delta$  (load factor):

$$F_e = \frac{m[V_s(R_s \cos \delta + X_{sd} \sin \delta) - E_f R_s]}{\omega_s(X_{sd}X_{sq} + R_s^2)} \quad (19)$$

The figure (3) shows the force-load factor characteristic ( $R_s=0$ ). Also, the efficiency can be calculated as follows [11]:

$$\eta = \frac{P_e}{P_{in}} = \frac{F_e \omega_s}{mV_s I_a \cos \varphi} \quad (20)$$

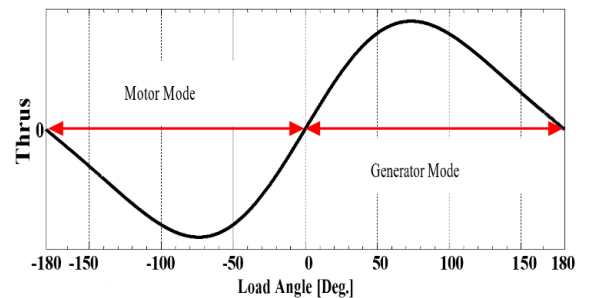


Fig. 2. Force-load factor characteristic for a motor with  $R_s=0$

#### IV. PROPOSED ALGORITHM FOR DESIGNING MOTOR

In this section, a new method for designing a Linear Synchronous Motor with DC excitation at the desired speed and thrust force will be presented. This method uses the steady-state model of the motor which is presented in the previous section.

##### A. Design of the Stator

Knowing the motor's speed, the pole pitch can be calculated from equation (14). Now the length of the motor is calculated from the following equation [11]:

$$L_s = 2p\tau \quad (21)$$

To have a proper rail, we should choose the proper length for the electrified area. The length of the electrified area can be considered as an integral coefficient of the length of the motor using the following relationship [12]:

$$L_{en} = k_{en}L_s \quad (22)$$

In the above equation,  $k_{en}$  is an integral coefficient. By increasing this coefficient, the active area will be increase, but the primary resistance will also increase, and this will cause more losses, and reduce efficiency. On the other hand, by choosing a small coefficient, the length of the active area will be reduced. Now, knowing the pole pitch and choosing the appropriate  $q$  (number of grooves in each phase in each pole), the groove pitch can be calculated from the following equation [11]:

$$\tau_s = \frac{\tau}{mq} \quad (23)$$

To calculate the dimensions of the groove, tooth width is considered as a coefficient of the groove pitch, and we have:

$$w_t = C_t \tau_s \quad (24)$$

Where,  $C_t$  is a coefficient between 0 and 1 because the width of the tooth is smaller than the pitch of the groove or is actually a part of the pitch of the groove. Now the width of the groove can also be calculated. To calculate the number of turns  $N_1$  and  $N_2$ , it is necessary to specify the number of turns in each coil ( $n_c$ ) and the number of pairs of poles. After choosing the type of winding, we first consider  $n_c$  equal to 1 and proceed with the calculations; If the thrust force obtained is at the desired level, we stop the calculations, otherwise, we increase  $n_c$ , and we repeat the calculations until the output thrust force is within the acceptable range. In this way, having  $n_c$  and choosing the type of winding for the motor, we will have:

$$N_1 = n_s p q \quad (25)$$

That,  $n_s$  is the number of conductors in each slot and it is obtained according to the type of winding. So:

- Single layer winding:

$$n_s = n_c \quad (26)$$

- Double layer winding:

$$n_s = 2n_c \quad (27)$$

And for  $N_2$ :

$$N_2 = k_{en} N_1 \quad (28)$$

To calculate the estimated current of the stator input ( $I_a$ ), the relation (20) is used:

$$I_a = \frac{F_{xd} \omega_s}{m V_s \eta \cos \varphi} \quad (29)$$

Where  $F_{xd}$  is the desired output thrust force. In this regard, to estimate the required input current to produce the desired thrust force, we must have the values of the input power factor and efficiency. For this purpose, we first assume that the product of two values is an arbitrary number between 0 and 1, after calculating the parameters of the circuit and obtaining the actual current of the motor, these values will be corrected. Now, by estimating the initial current and selecting the allowed current density for the primary winding, the cross section of the groove can be calculated. With the groove's width and cross section values, the height of the groove can be calculated. By considering the proper coefficients (such as the Carter's coefficient) for the electrical relations, that presented in the previous section, the electrical parameters of the motor can be calculated. By calculating these parameters and applying the relations (1) and (2) and using the phasor diagram of the real input current can be calculated. It should be noted that the suitable angle of the load can be calculated according to the characteristic force-load angle according to equation (19). To calculate  $E_f$  in the mentioned equations, first we choose a value for the flux density of the stator tooth according to the magnetization curve of the iron, which used in the stator core. First, by ignoring the effect of the armature on the air gap's flux density, the upper limit for the air gap's flux density caused by DC excitation can be obtained from equation (15). With the appropriate choice for this flux density, the induced voltage  $E_f$  can be calculated.

It should be noted that this is a suitable choice because the main flux of the motor is the same flux caused by DC excitation, and the changes in the electrical characteristics of the stator will not change much in this flux density. Of course, it should be noted that at the end, the actual value of the air gap's flux density will be obtained by considering the effect of the armature, and accordingly, the actual flux density of the stator teeth. Now, with the determination of the actual current of the motor, the power factor can be calculated using the relations (1), (2), and using the phasor diagram, and the efficiency from the relation (20). By calculating the actual values of the power factor and efficiency, the actual value of the product of these two values can be calculated. If this real value is within the acceptable range of the initially selected value, we stop the calculations for this section, and if not, a new selected value is determined according to the following relationship and we repeat the calculations to reach convergence for this value:

$$(\eta \cos \varphi)_{new} = \frac{(\eta \cos \varphi)_{cal} + (\eta \cos \varphi)_{es}}{2} \quad (30)$$

Now the output thrust force is calculated; If the difference between the obtained value and the desired thrust force is acceptable, we stop the calculations, and if not, put  $n_c+1$  instead of  $n_c$  and repeat the calculations until the desired value for the thrust force is obtained. At the end, by determining the number of turns in each coil, the number of turns in each phase, the corresponding initial current and the cross-sectional area obtained for the conductors, the desired wire is selected from the standard table. According to the diameter of the selected conductor, the width of the groove and tooth should be recalculated. By calculating the width of the groove and tooth, the flux density in the teeth is calculated from relations (15) and (16) and compared with the maximum value. If the value of the obtained flux density is higher than its default

value, the tooth width should be increased. At the end, the output parameters of the machine and the weight of its

different parts are recalculated. The block diagram of this method is shown in Figure 3.

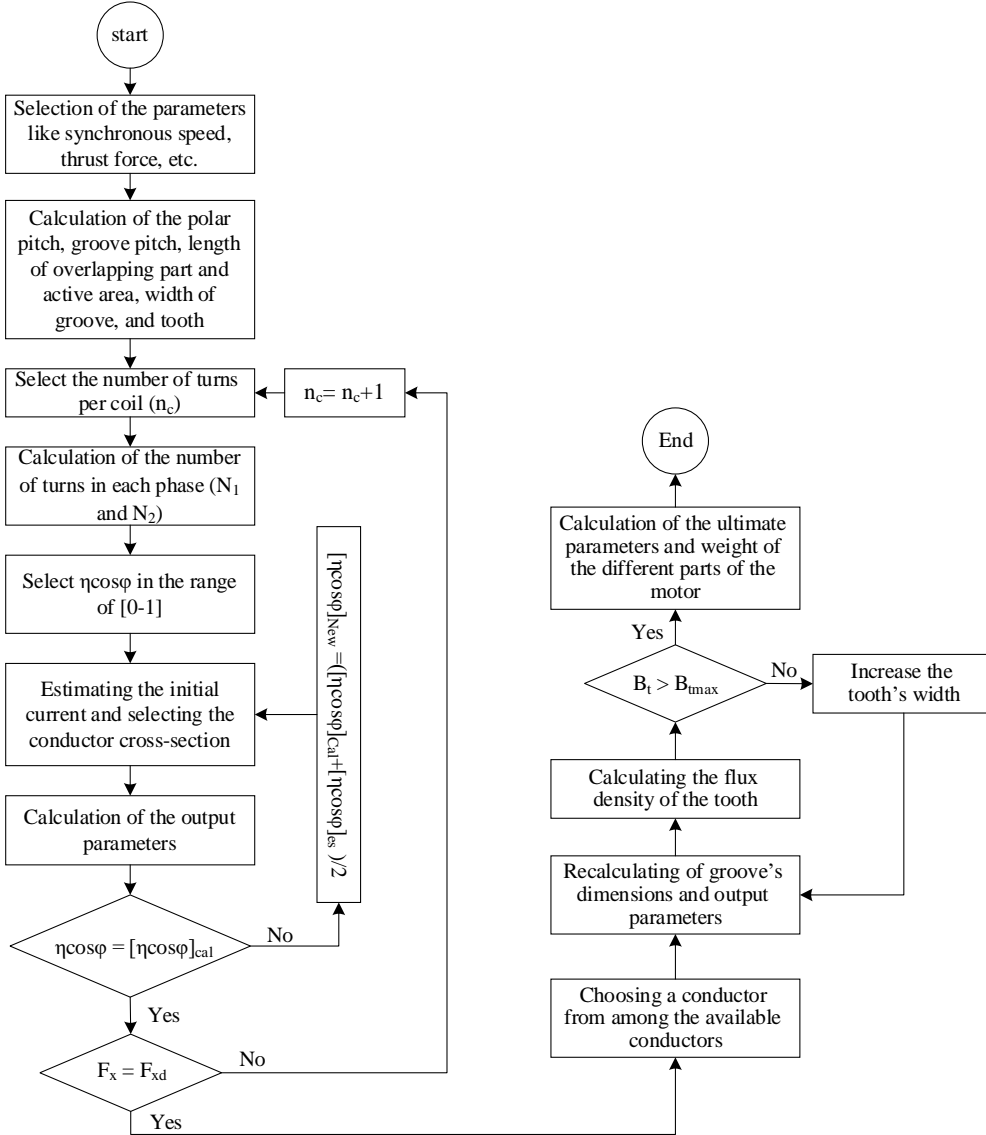


Fig. 3. Block diagram of the proposed method

### B. Design of the Rotor

Now, by designing the stator and obtaining the required air gap flux density, it is possible to calculate the  $W_f I_f$  using equation (12). By using equations (13) and (14), other parameters of the DC excitation circuit can be calculated.

### C. Optimization

In order to provide proper optimization, the machine's sensitivity to changes in parameters such as frequency, machine width, and air distance is first examined. These studies are shown in Figures 4 to 6. As the frequency increases, the polar pitch decreases. The primary resistance will decrease due to the direct relationship with the polar pitch, and on the other hand, the primary reactance will increase with the increase in frequency. With these explanations and precision in Figure 4, we will see that the input current increases initially with the decrease of the resistance and then decreases with the increase of the reactance. Accordingly, the power also increases at first and then decreases. Also, the downward trend of the power factor can be seen. Efficiency is

also improved by reducing initial resistance and reducing losses. Increasing the width of the machine to specific points for power, power factor, and efficiency brings an upward trend, which can be seen in Figure 5, which is caused by changes in the induced voltage and the angle of the input current with this voltage. Figure 6 shows that choosing a small air gap improves the machine's output parameters on the other hand, in applications such as magnetic trains, reducing the air gap is limited due to high speeds and the possibility of the train hitting the rail. The power to reduce the air gap too much. Of course, parameters such as load angle and tooth width were also investigated, but due to the limitation in the number of pages, only their optimization results are given.

The Particle Swarm Optimization (PSO) algorithm has optimized the design [1]. This article uses the normalized multiplication of individual cost functions to convert multi-objective optimization into single-objective optimization. Once the weight cost function is considered, first, the inverse normalized cost functions of rail weight per unit length and

moving weight are added together and considered a cost function. This cost function can be expressed as follows:

$$M = f_{u1} \times f_{u2} \times f_{u3} \times f_{u4} \quad (31)$$

Where  $f_{u1}$ ,  $f_{u2}$ , and  $f_{u3}$  are the desired objective functions for propulsion force, power factor, and efficiency, respectively.  $f_{u4}$  is also the objective function for choosing the minimum rail weight per unit length and moving weight, which is presented below how to calculate it:

$$f_{u4} = \frac{\left(\frac{1}{W_{metr}} + \frac{1}{W_{tp2}}\right)}{2} \quad (32)$$

In the above relationship,  $W_{tp2}$  and  $W_{metr}$  are the weight of moving and the weight per unit of rail length, respectively.

The optimized values of the desired parameters and each range are shown in Tables I and II.

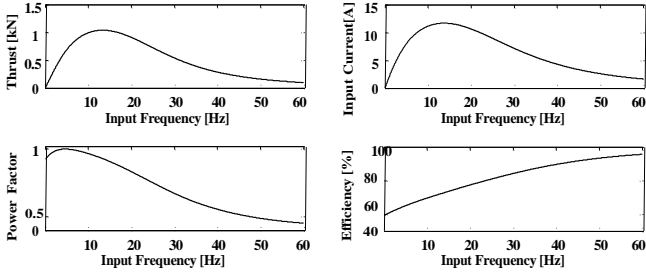


Fig. 4. The effect of input frequency on the motor's output parameters

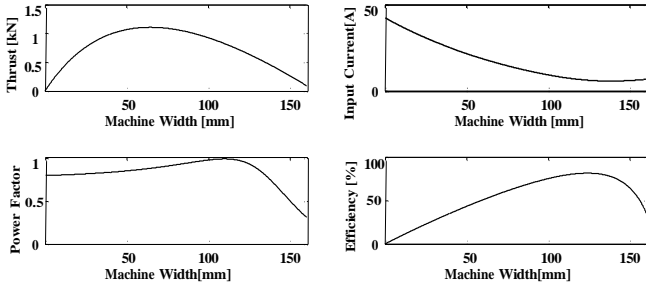


Fig. 5. The effect of machine width on the motor's output parameters

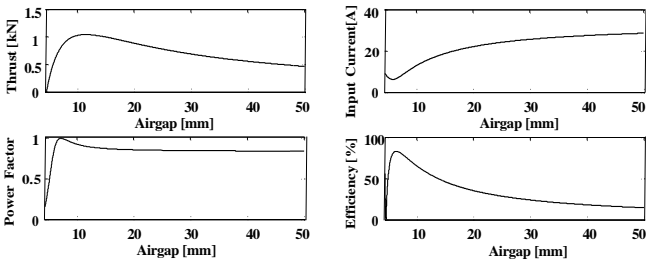


Fig. 6. The effect of airgap on the motor's output parameters

## V. VERIFICATION

To validate the results which obtained from the design presented in the previous section, a motor with the specifications in table I was designed with the proposed method, and the circuit parameters obtained from this method were simulated with the Finite Element Method. ©Maxwell was used for this simulation. The results of the simulation are shown in Figures 7 to 10. According to the rail's constraints, the initial speed and weight are considered 5 m/s (synchronous and 1 kg, respectively). The figure 7 shows the motor's speed. According to figure 7, after 100 ms, the speed of the motor

reaches the synchronous speed. Figure 8 shows the motor's tractive force at nominal load. As can be seen in the figure 8, the average output power is 953.42 N. Figures 9 and 10 show the input current and voltage, respectively. Also, the distribution of the flux density is shown in Figure 11. In Figure 11, it can be seen that the maximum flux density occurs in the yoke and it is equal to 2T.

TABLE I. MACHINE PARAMETERS FOR OPTIMIZATION AND THEIR RANGE OF CHANGES

Parameters	Unit	Range of changes (Max-Min)	Optimization value
Frequency	Hz	100-10	10.8
Number of slots/poles/phases	-	2-1	2
Motor's width	mm	200-20	90
Airgap	mm	30-10	10.6
Groove width/Groove pitch	-	0.5-0.3	0.5
Load's angle	degree	180-0	12.75

TABLE II. OPTIMIZATION RESULTS FOR THE DESIRED OBJECTIVE FUNCTIONS

Parameters	Unit	Optimization results
Thrust force	N	953.42
Power factor	-	0.932
Efficiency	[%]	71.7
Rail weight per unit length	Kg/m	86.96
Moving's weight	Kg	480.364

For a better comparison between the output results of two methods at the nominal load, it is displayed in Table III. In this table, the error is calculated as follows:

$$\text{Error} = \frac{\text{FEM results} - \text{Calculated results}}{\text{FEM results}} \quad (33)$$

As it is manifest from Table III, the induced voltage predicted by the proposed method is slightly higher than the actual value, which means that the air gap is smaller than the actual value. With this analysis, it can be expected that the current is slightly lower than the actual value predicted.

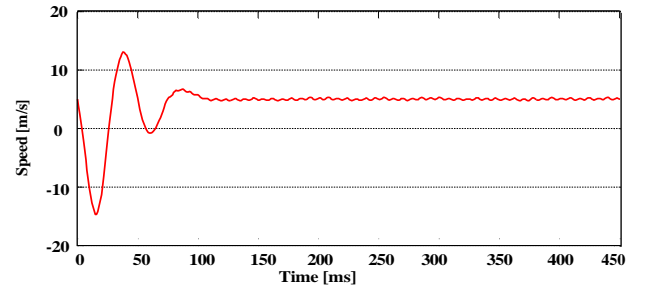


Fig. 7. The speed obtained from the finite element

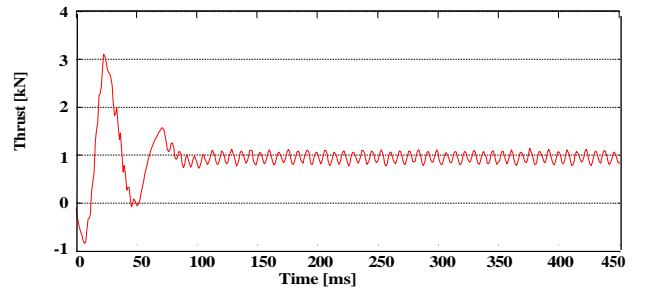


Fig. 8. The output force obtained from the finite element method

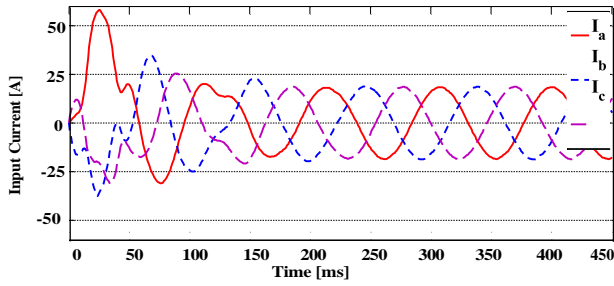


Fig. 9. Input current obtained from finite element method

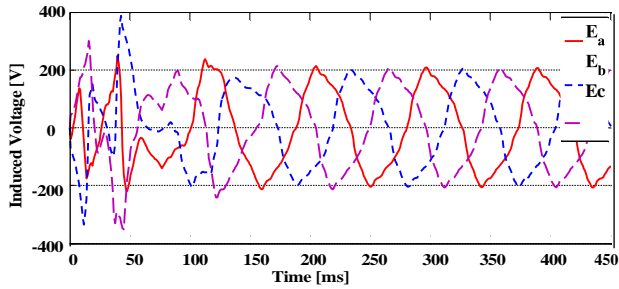


Fig. 10. Induced voltage on the stator phases obtained from the finite element method

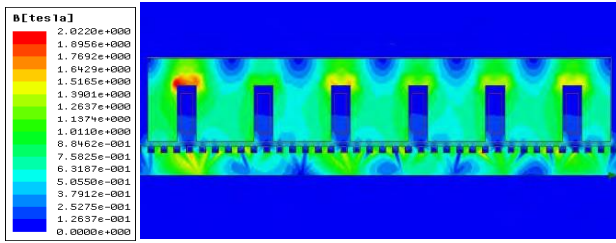


Fig. 11. Distribution of the flux density in different parts of the motor

TABLE III. COMPARISON OF THE OUTPUT RESULTS FOR THE PROPOSED METHOD AND THE FINITE ELEMENT METHOD

Parameters	Unit	Results of the proposed method	Results of the FEM	Error [%]
Thrust force	N	953.42	953.42	0
Input Current	A	10.82	13.06	17.2
Induced Voltage	V	153.01	148.98	-2.7
Power factor	-	0.932	0.898	-3.78
Efficiency	[%]	71.7	65	-10.3

## VI. CONCLOTION

In this article, a method was presented for designing a linear synchronous motor based on steady state equations. In the previously presented methods, electromagnetic equations or numerical methods such as finite element methods, are usually used, which in addition to complexity, are time-consuming and not suitable for optimization. This is despite the fact that the presented method solves the mentioned problems and can be used in sensitivity analysis and optimization. The finite element method was used to validate the design's results, and its results confirm the results of the presented method.

## REFERENCES

- [1] A. Mousaei and M. B. B. Sharifian, "Design and optimization of a linear induction motor with hybrid secondary for textile applications," 2020 28th Iranian Conference on Electrical Engineering (ICEE), 2020, pp. 1-6, doi: 10.1109/ICEE50131.2020.9260773.
- [2] Gieras, Jacek F., Zbigniew J. Piech, and Bronislaw Tomczuk. Linear synchronous motors: transportation and automation systems. CRC press, 2018.
- [3] A. Mousaei, M. B. Bannae Sharifian and N. Rostami, "An Improved Fuzzy Logic Control Strategy of an Optimized Linear Induction Motor Using Super Twisting Sliding Mode Controller," 2022 13th Power Electronics, Drive Systems, and Technologies Conference (PEDSTC), 2022, pp. 1-5, doi:10.1109/PEDSTC53976.2022.9767465.
- [4] Akita, Soei, et al. "Design analysis of a line-start permanent magnet linear synchronous motor." 2017 11th International Symposium on Linear Drives for Industry Applications (LDIA). IEEE, 2017.
- [5] A. Mousaei, M. B. Bannae Sharifian and N. Rostami, "An Improved Predictive Current Control Strategy of Linear Induction Motor Based on Ultra-Local Model and Extended State Observer," 2022 13th Power Electronics, Drive Systems, and Technologies Conference (PEDSTC), 2022, pp. 12-18, doi:10.1109/PEDSTC53976.2022.9767535.
- [6] Boldea, Ion. Linear electric machines, drives, and MAGLEVs handbook. CRC press, 2017.
- [7] A. Mousaei, M. B. Bannae Sharifian and N. Rostami, "Direct Thrust Force Control (DTFC) of Optimized Linear Induction Motor with Super Twisting Sliding Mode Controller (STSMC)," 2021 12th Power Electronics, Drive Systems, and Technologies Conference (PEDSTC), 2021, pp. 1-5, doi: 10.1109/PEDSTC52094.2021.9405903.
- [8] Tavana, Nariman Roshandel, and Venkata Dinavahi. "Design of slotted permanent magnet linear synchronous motor for improved thrust density." 2013 International Electric Machines & Drives Conference. IEEE, 2013.
- [9] Arash Mousaei, Nasim Bahari, Guo Mieho. Artificial Neural Networks (ANN) of Proposed Linear Induction Motor with Hybrid Secondary (HLIM) Considering the End Effect. American Journal of Electrical and Computer Engineering. Vol. 5, No. 1, 2021, pp. 32-39. doi: 10.11648/j.ajece.20210501.15.
- [10] Hwang, Chang-Chou, Ping-Lun Li, and Cheng-Tsung Liu. "Optimal design of a permanent magnet linear synchronous motor with low cogging force." *IEEE Transactions on Magnetics* 48.2 (2012): 1039-1042.
- [11] A. Shiri and A. Sholai, "Linear Induction Motor, Analysis, Design and Modeling", Shahid Rajaee University Press Education, Fall 2016.